J Therm Anal Calorim (2015) 122:579–588
DOI 10.1007/s10973-015-4734-6

A three-step synthesis process of submicron boron carbide powders using microwave energy

M. R. Forouzan[1] · R. Taherzadeh Mousavian[2] · T. Sharif[3] · Y. A. Afkham[4]

Received: 11 November 2014 / Accepted: 30 April 2015 / Published online: 27 May 2015

Abstract In this study, a three-step synthesis process is proposed for the production of submicron B_4C powders. The initial step is the mechanical activation of a Mg–C–B_2O_3 mixture, which is carried out by using a high-energy planetary ball mill. The second phase is the microwave-assisted combustion synthesis, used to fabricate the MgO–B_4C composite powders. The final stage is an acid leaching for removing the MgO phase. The results of DSC, XRD, and SEM analyses indicated that mechanical activation was a vital process for microwave synthesis and that no starting powders were remained unreacted after microwave heating. A considerable reduction in reaction temperature was obtained from DSC analysis after mechanical activation process. TG results indicated that separated milling of Mg with B_2O_3 powders would avoid the formation of gases during exothermic reactions. Finally, it was found that submicron boron carbide powders with an average crystallite size about 114 nm were produced with a high purity after acid leaching.

Keywords Boron carbide · Microwave-assisted combustion synthesis (MACS) · Mechanical activation · Ball milling

✉ R. Taherzadeh Mousavian
rtaher1898@gmail.com; r_taherzadeh@sut.ac.ir

[1] Department of Materials Science and Engineering, Shiraz University, Shiraz, Iran

[2] Young Researchers and Elite Club, Ilkhchi Branch, Islamic Azad University, Ilkhchi, Iran

[3] Department of Metallurgy, Karaj Branch, Islamic Azad University, Karaj, Iran

[4] Faculty of Materials Engineering, Sahand University of Technology, Tabriz, Iran

Introduction

Boron carbide is a solid solution stable over the compositional range of 8.9–24.3 at.% C. Its noticeable properties are highest hardness over 1100 °C, high strength, high melting point (2450 °C), low density (2.52 g cm^{-3}), good wear resistance, good chemical stability, high Young modulus (457 Gpa), and high resistivity at elevated temperatures. Due to its high hardness, boron carbide powder is used as an abrasive in polishing, ball mills, nozzles for slurry pumping, sand blasting nozzles, grinding media, ceramic bearing, wire drawing dies, lapping applications, and also as a loose abrasive in cutting applications such as water jet cutting [1–6].

A number of processes are available for the synthesis of B_4C powders, and each process varies in the characteristics of the powder produced and processing cost. Recently, some authors reported that B_4C ceramic powder could be formed via magnesiothermic reduction process using boron sources such as B, B_2O_3, H_3BO_3, and $Na_2B_4O_7$, as well as Mg and carbon sources such as petroleum coke, graphite, and activated carbon [7–16]. Magnesiothermic reduction process could be formed using mechanochemical synthesis using a ball milling or self-propagation high-temperature synthesis (SHS) process. Sharifi et al. [8] reported the formation of B_4C nanoparticles using mechanochemical synthesis. Deng et al. [15] synthesized submicron-sized boron carbide particles by the reduction of boron oxide with carbon and magnesium by mechanical alloying method using a planetary ball mill. The advantages of ball milling (mechanochemical synthesis) are easy handling, and the applicability to a wide range of different classes of materials [17, 18]. However, due to a long time needed for the production of a low amount powders, the process is not economical and it seems that it could not be scaled to an

industrial level. In addition, due to the long milling times (tens and even hundreds of hours), the final products become contaminated by substances erased from the walls of mill vials and balls. Thus, the drawbacks of this process lie in high-energy consumption and low product purity [19–22]. SHS process has been used so far as an inexpensive process, in which highly exothermic reactions between the constituents become self-sustaining and proceed via a combustion propagation wave through an entire sample, providing an attractive low cost alternative to conventional methods of producing advanced materials [23–27]. It should be noted that these exothermic reactions could be simply confined using diluents, etc., to avoid damaging the combustion chamber. Siegert et al. [28] have reported that the addition of significant amounts of carbon into thermite compositions, by enclosing the oxide into hollow carbon fibers, slows down the propagation velocity of the combustion front, due in particular to the separation of the reactive phases by the carbon walls and to the formation of carbide. The energy-efficient nature of the process stems from the fact that the energy required is provided by the reaction enthalpy. An external energy source is only used for local ignition of reactant powders or a compact on one end. Once initiated by a hot wire, the external heat source is turned off immediately and the process requires no further addition of energy. The process is simple and lacks a need for complicated expensive experimental configurations. The reaction is complete within seconds rather than hours, which makes SHS an economical process [29, 30]. The chemical reaction of the mixture of B_2O_3 and C reacted with Mg to produce B_4C is shown in Eq. (1) [14]:

$$B_2O_3 + 0.5C + 3Mg = 0.5B_4C + 3MgO \quad (1)$$

When Mg is selected as the reducing agent, the leaching process of the SHS product should be carried out in HCl containing aqueous media to obtain clean boride product on a filter. MgO dissolution reaction in an aqueous HCl solution is shown in Eq. (2) [14].

$$MgO(s) + 2HCl(aq) = Mg^{2+}(aq) + 2Cl^{-}(aq) + H_2O(l) \quad (2)$$

Recently, it has been reported that microwave energy can be used to synthesize ceramic powders where reactions of component oxides at elevated temperatures are involved [27, 31–34]. Microwave-assisted combustion synthesis (MACS) technique has been effectively used to produce powders in shorter times in comparison with the conventional synthesis carried out in an electric furnace [27, 35, 36]. Microwave synthesis of materials is fundamentally different from the conventional synthesis in terms of its heating mechanism. In a microwave oven, heat is generated within the sample volume itself by the interaction of microwaves with the material [37, 38]. Microwave energy heats the material on a molecular level, which leads to uniform heating, whereas conventional heating systems heat the material from outer surface to interior, which results into steep thermal gradients. In fact, microwave energy has became an essential tool in the processing of some of the technologically important products such as ceramic honeycombs, where thermal gradients have to be minimized in order to avoid the formation of cracks which occur during drying [27, 37, 38].

In this study, the formation of submicron-sized boron carbide powders was studied via MACS technique using a graphite–boric acid–Mg mixture.

Experimental

Samples preparation

The materials used in this study were 99 % pure graphite powder, 99.5 % pure Mg powder, and 99 % pure H_3BO_3 powder. B_2O_3 was obtained by the calcination of 99 % pure boric acid at 130 °C for 4 h. Based on Eq. (3) and molar mass values of boric acid, boron oxide, and water, about 44 % mass loss should be occurred after complete calcination of boric acid:

$$2H_3BO_3 \rightarrow B_2O_3 + 3H_2O \quad (3)$$

It was found in our examinations that a gelatin-like material would be obtained after boric acid calcination if the temperature is higher than 150 °C. This causes the boric acid powders not to easily convert to boron oxide and an extensive adhesion to the container wall is occurred. However, it was found that 4-h heating at 130 °C is necessary for complete conversion of boric acid to boron oxide. After this process, about 46 % mass loss was calculated that was higher than the required amount needed for complete calcination, for which the removal of impurities from the boric acid powders might be responsible in this regard.

The morphology of starting powders as well as their average particle size is shown in Figs. 1 and 2, respectively. The graphite powder is angular and flaky in shape with a mean particle size of 40 μm, while the Mg powder has two averages particle size of about 80 and 250 μm. Dried B_2O_3 powders has an irregular shape of about 10 μm in mean diameter size. During the process, the boric acid powders were continuously blended to be sure about the complete conversion to boron oxide. Two samples were fabricated in this study to investigate the effect of mechanical activation on the reaction mechanism. Table 1 shows how these two samples were prepared in this study. As can be seen, sample S_1 is just milled for 5 min to obtain a minimum required interface between the starting powders. It should be noted that before mechanical activation

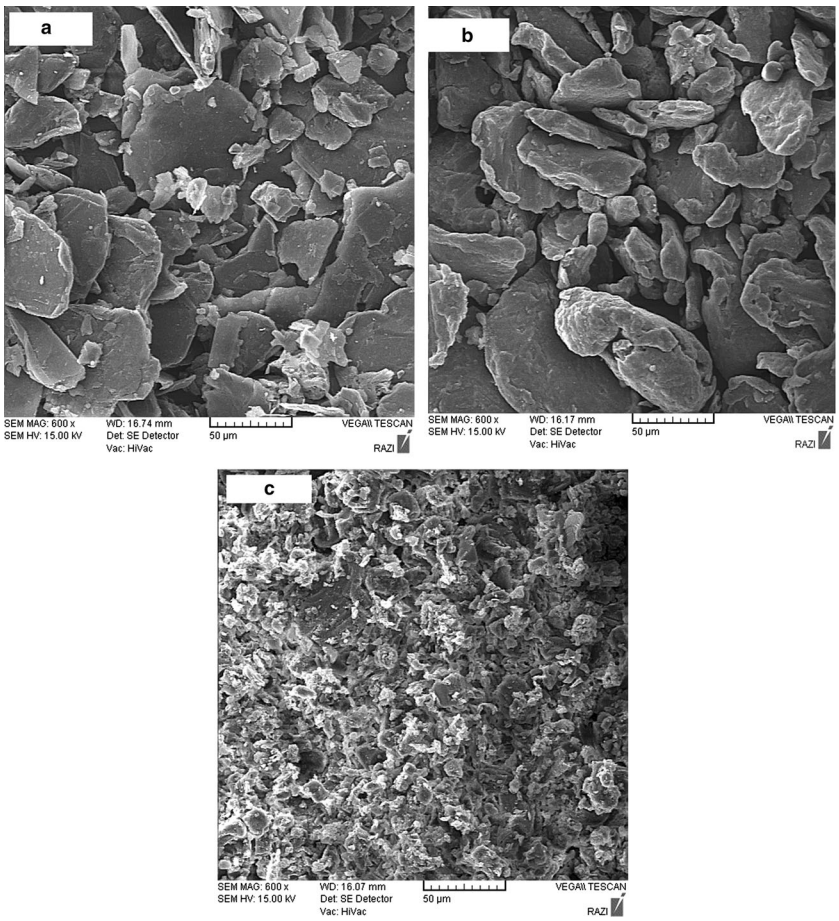

Fig. 1 Scanning electron micrographs of images of as-received powders, **a** graphite, **b** Mg, **c** dried boric acid

process for sample S_2, to avoid CO or CO_2 formation, B_2O_3 and Mg powders were separately mixed and milled with each other in accordance with the needed calculated mass based on reaction (1). The graphite powders were then added to this mixture based on reaction (1) (to the best of our knowledge, this method is novel). All the milling processes were performed under argon atmosphere (with purity of 99.99 %) by using a Fritsch Pulverisette P5 planetary ball mill using steel vial and a blend of hardened steel balls (6 g 10 mm and 94 g 20 mm diameters, total balls mass: 100 g). Both the samples were then uniaxially pressed without a binder at 400 MPa pressure into a disk of 15 mm diameter and 5 mm height to approximately 70 % of the theoretical maximum density (TMD). The cold-pressed specimens were placed inside a quartz tube (inside diameter: 25 mm). The quartz tube was surrounded with Al_2O_3 fiber blocks in order to minimize heat loss. The quartz tube was purged with argon continuously at a flow rate of 2 L min^{-1} during heating. They were then put in a domestic microwave oven (LG Electronics Inc., 1.0 kW power and 2480 MHz frequency) for the MACS process. A provision was made for the escape of combustion gases via quartz tube by providing two exhaust openings at the top of the microwave oven. After MACS process and crushing of the synthesized samples, MgO and the other unwanted products were leached out by hot hydrochloric acid for 1 h at 110 °C using an enclosed container to avoid evaporation of the solution. The solution was filtered after leaching, and the purified products were washed by distilled water for several times to eliminate extra HCl acid. The purified products were then dried in oven at 70 °C for 1 h.

Samples characterization

The physio-chemical changes for both the samples during heating were investigated by a simultaneous TG/DSC measurement using a Netzsch STA 409 (Germany) analyzer with a maximum working temperature of 1500 °C to study the effects of mechanical activation on the reactions. The TG/DSC experiments utilized high-purity corundum as a reference. Powder samples of $\approx$30 mg were loaded and pressed into an alumina crucible, which will not react with the reactants, and heated up in an inert argon atmosphere at the rate of 20 °C min^{-1}. The phase

compositions of the samples before MACS as well as those of crushed powders after MACS and leached products were characterized by using X-ray diffractometer (Bruker's D8 advance system, Germany) using CuKα ($\lambda = 0.15405$ nm) radiation. The crystallite size analysis was made through X-ray diffraction (XRD) patterns using the Scherrer method [39, 40].

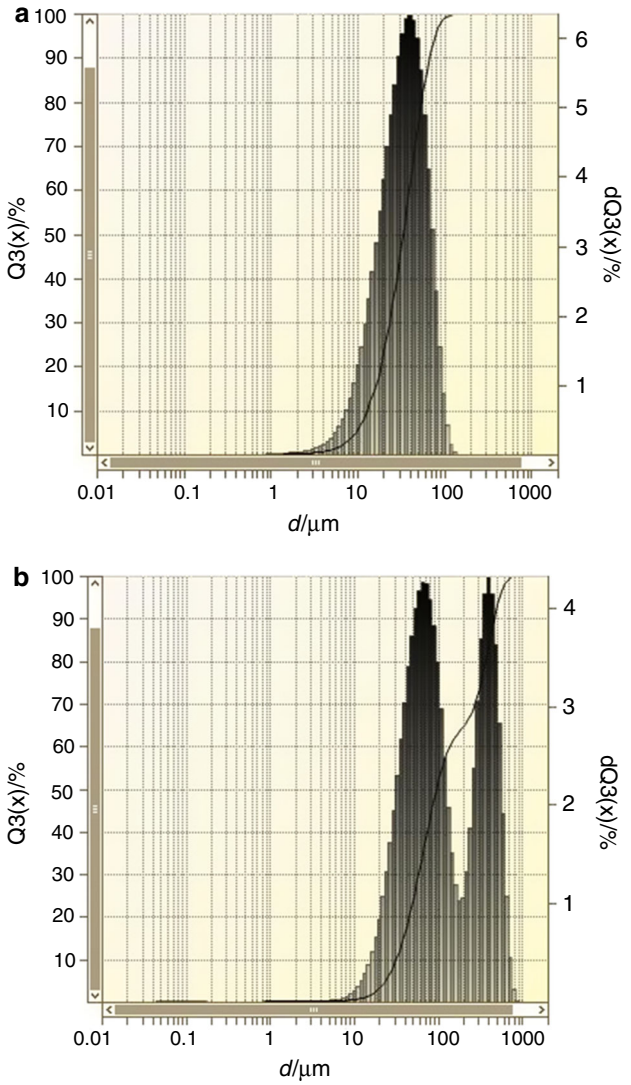

Fig. 2 Particle size distribution of the starting powders, graphite (**a**), Mg (**b**)

$$D = K\lambda/(\beta \cos \theta) \quad (4)$$

where θ is the Bragg diffraction angle, K is a dimensionless shape factor, D is the average crystallite size, λ is the wavelength of the radiation used, and β is the line broadening at half the maximum intensity (FWHM), after subtracting the instrumental line broadening, in radians.

The microstructures of the as-milled and as-synthesized powders were studied using two kinds of scanning electron microscopes (SEM, Cam Scan Mv2300 and KYKY-EM3200). The specific surface areas and mean particle size of the B_4C powders after leaching were measured from the nitrogen absorption data using the Brunauer–Emmett–Teller (BET) technique (Quantachrome Nova 2200e) and laser particle size analyzer (Mastersizer 2000, Malvern), respectively.

Results and discussion

Figure 3 shows the XRD pattern of the samples. As this figure shows, no phase composition change has occurred after mechanical activation of the powders, meaning that no reaction has occurred, although Mg and B_2O_3 powders were previously milled separately for 1 h and then mixed together. As can be seen, some corresponding peaks of the starting powders have disappeared after mechanical activation. The background is also increased after 5-h mechanical activation. This slight peaks disappearing is usually associated with combined instrumental effects and structural factors such as reduced crystallite size, and strain at the atomic scale caused by the lattice distortion [21]. In addition, despite the XRD results, the possible oxidation of Mg powders in some parts due to their exposure to the boron oxide powders during the first step of milling might be the other reason for disappearing of some corresponding peaks of the starting powders. The XRD analysis could not detect the phases with low amount of volume fraction.

Figure 4a shows the X-ray phase analysis of the crushed powders after MACS process. As it indicates, MgO phase is a dominant phase, which was fabricated as well as B_4C phase. No other phases could be obtained after MACS, meaning that mechanical activation was high enough for these powders to react with each other after heating in the microwave. Our results indicated that no combustion

Table 1 Ball milling parameters of the samples

Sample	Step 1	Step 2
S_1	5-min mixing of Mg, B_2O_3, and graphite powder with the rotating speed of 400 rpm and ball-to-mass ratio of 5:1	–
S_2	Milling of B_2O_3 and Mg powders for 1 h with the rotating speed of 400 rpm and ball-to-mass ratio of 5:1	Addition of graphite to the milled powders of step 1 (B_2O_3 + Mg) and milling them (C + B_2O_3 + Mg) for 4 h with the rotating speed of 400 rpm and ball-to-mass ratio of 5:1

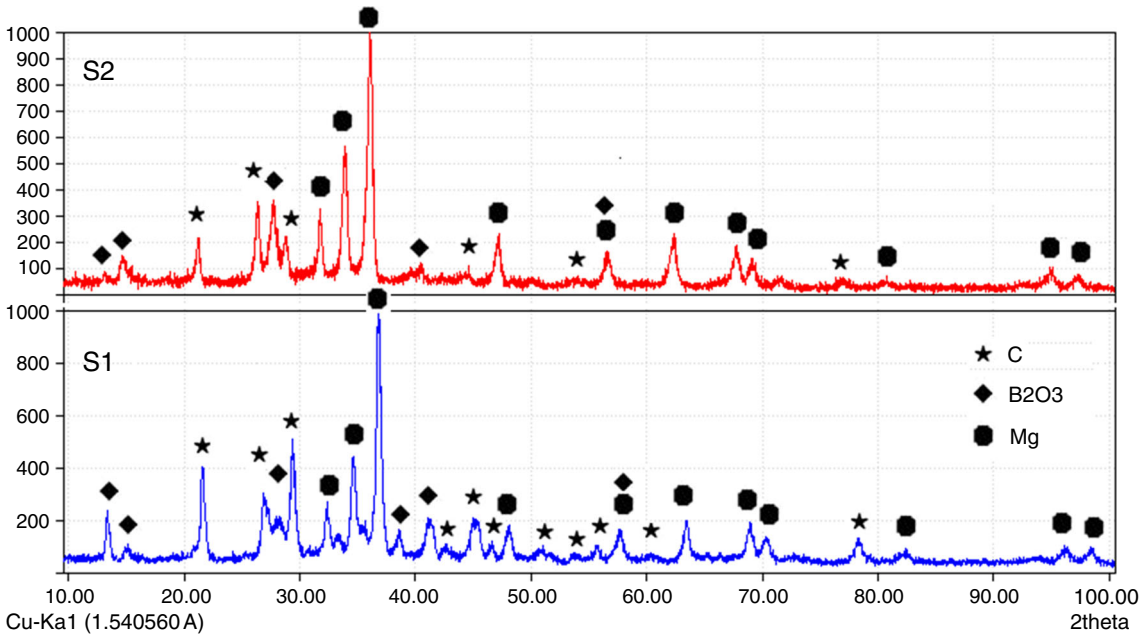

Fig. 3 XRD patterns of samples S_1 and S_2 before MACS process

synthesis was happened after MACS for sample S_1, meaning that even a high rate of heating in the microwave could not stimulate the as-mixed powders to start the reaction. Therefore, no phase change was observed for the sample S_1 after MACS. Another important result was that the amount of existing gases from the microwave oven was considerable for sample S_1. Generally, the complete reaction of the carbon is very difficult because the reaction by-product such as carbon monoxide carries volatile boric species away from the reaction site, which breaks the stoichiometry [41, 42]. It seems that milling of B_2O_3 and Mg powders followed by mechanical activation process for 4 h could lead to the prevention of unwanted intermediate products formation during MACS. After leaching of the crushed milled powders, the XRD analysis was applied to investigate whether MgO was removed after acid leaching. As it can be seen in Fig. 4b, no peaks corresponding to the other products could be seen beside B_4C phase. The B_4C phase peaks seem to have a low intensity and a high width, and the results of crystallite size calculation based on the Scherrer equation indicated that the produced B_4C phase has an average determined crystallite size value of 114 nm.

Figure 5 shows the as-mixed sample S_1 (left image) and mechanically activated sample S_2 (right image), which were exposed to the microwave heating. As it can be seen, no distortion could be seen for the as-mixed sample S_1, while it seems that intensive reactions have occurred during MACS for sample S_2 containing mechanically activated powders.

As just 5-min milling was applied for the sample S_1 and no considerable morphological change was obtained for the starting powders, therefore SEM analysis was only performed for sample S_2. Figure 6a shows the powders' morphology of sample S_2 before MACS. It seems that a considerable agglomeration has occurred for the Mg–B_2O_3–C milled mixture. The brittle nature of boron oxide powders led to fragmentation of these powders, and it could be seen that submicron-sized B_2O_3 particles with round shape were embedded in a ductile matrix of Mg and graphite, leading to an adequate interface between the starting powders. However, it should be mentioned that the agglomeration of B_2O_3 fine powders (see Fig. 6a) is inevitable during milling and an ideal distribution of the starting powders will not be obtained during ball milling. It seems that ductile powders (graphite and Mg) with larger particles size and sheet-like morphology might be well embedded the brittle fine B_2O_3 powders (see Figs. 1 and 2). In fact, for making a suitable contact between the starting powders for complete reactions, the morphology and the particle size of starting powders are the important factors. Figure 6b shows the morphology of the crushed sample S_2 after MACS using a ball mill for 10 min. A brittle nature could be seen due to a formation of edge-like fine powders after considerable fracturing during just 10-min crushing. The powders are appeared to be fine in average particle size. The XRD patterns (see Fig. 4a) indicated that these powders were composed of MgO and B_4C phases.

Figure 7 shows the morphology of B_4C powders after acid leaching. Ultra-fine B_4C powders were produced with almost a spherical shape after acid leaching; Fig. 8 indicates that their average particle size ($d_{0.5}$) is about 0.669 μm, while their specific surface area is about

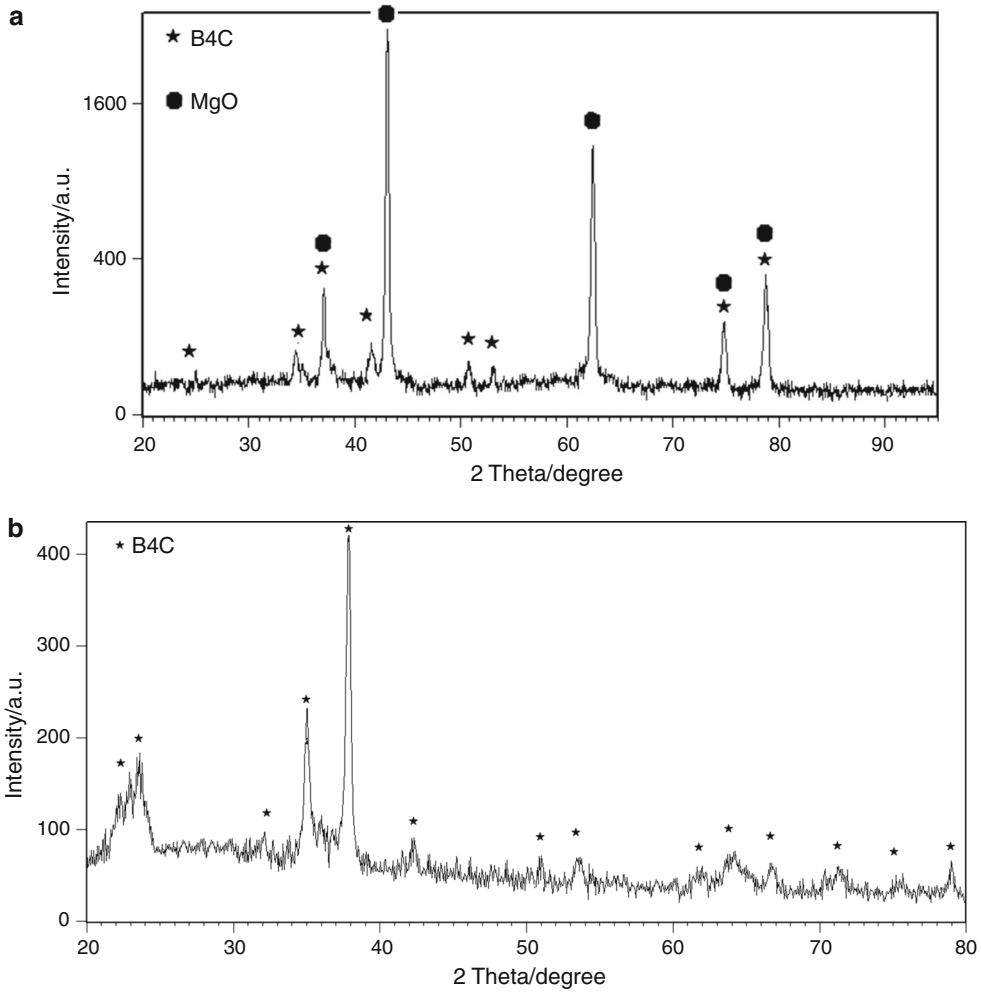

Fig. 4 XRD patterns of sample S_2 after MACS (**a**) and acid leaching (**b**)

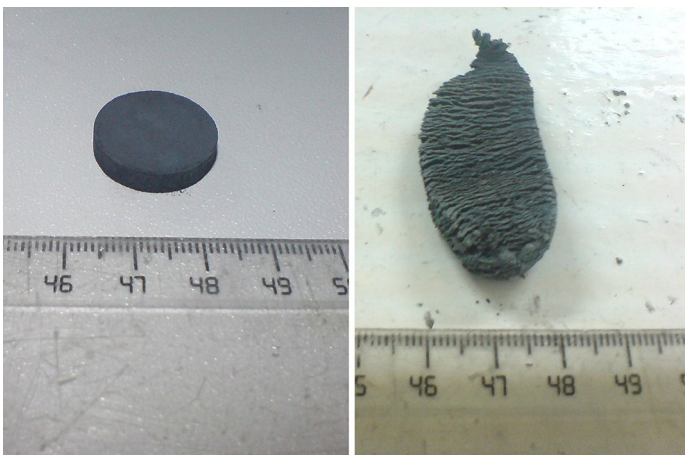

Fig. 5 Images of samples S_1 (*right image*) and S_2 (*left image*) after MACS process

10 m^2 g^{-1}. As can be seen in Fig. 7, the powders have a diameter size below 3 μm. In fact, it seems that a much lower particle size was obtained for the B_4C powders in respect to that shown in Fig. 6b, indicating that the presence of MgO phase caused the particle sizes of the B_4C–MgO mixed powders to have a higher average particle size. This means that acid leaching that removed the MgO phase, which seems to behave like cement toward

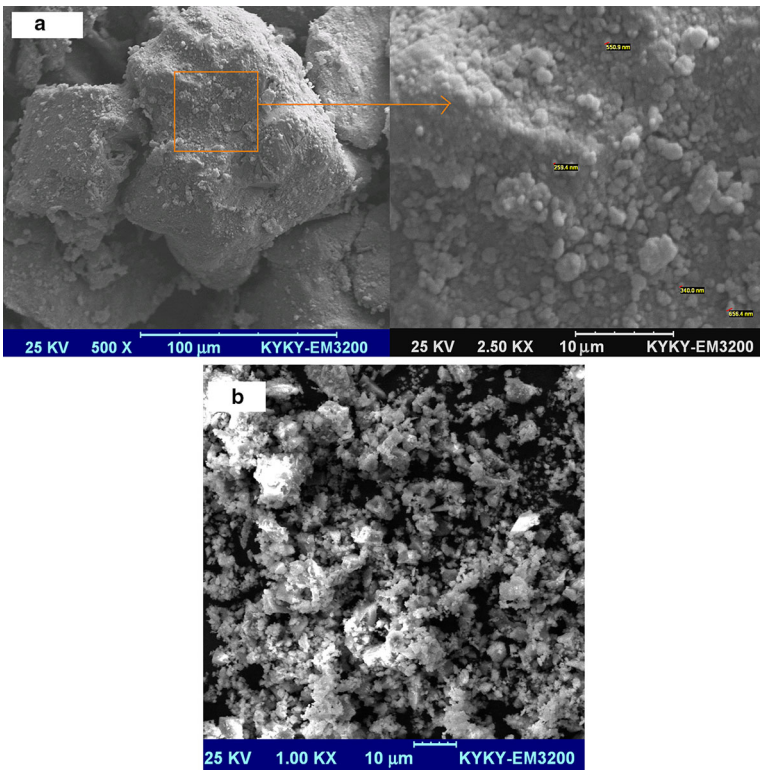

Fig. 6 SEM images of powders of sample S_2 before (**a**) and after MACS (**b**)

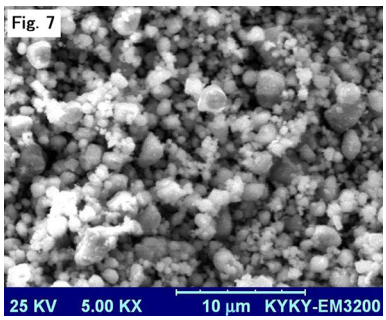

Fig. 7 SEM image of B_4C powders obtained after acid leaching

B_4C particles, led to the formation of pure B_4C phase with a lower average particle size.

High-energy collisions between the reactant powders and balls inside a ball mill could lead to the mechanical activation of the powders, which may enhance the kinetic of the reactions as a result of the mixing and refining of the microstructure and increase the energy level of the starting powders, allowing the reaction to occur at much lower temperatures than normally required [26, 30, 43–46]. Figure 9a shows the DSC/TG analysis of as-mixed powders of sample S_1, which were exposed to heating up to 1000 °C. As can be seen, two successive endothermic peaks were

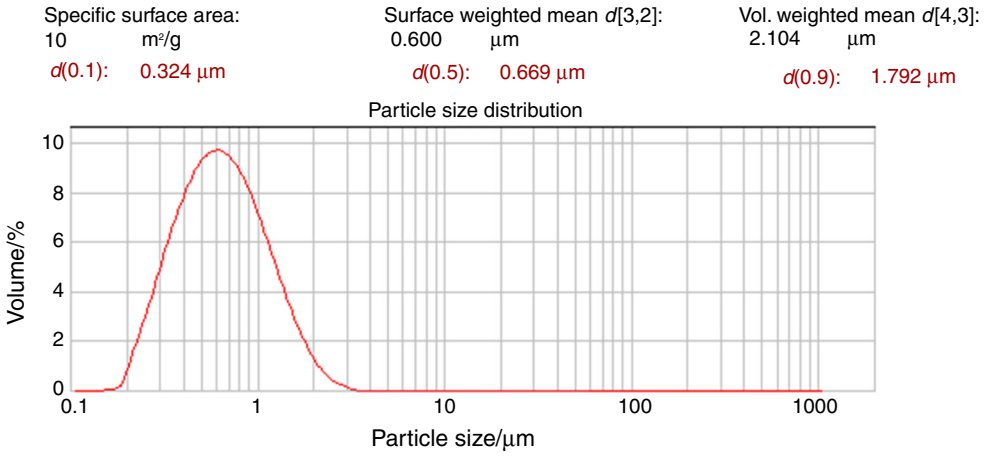

Fig. 8 Particle size distribution and surface area of B4C powders measured by laser granulometry

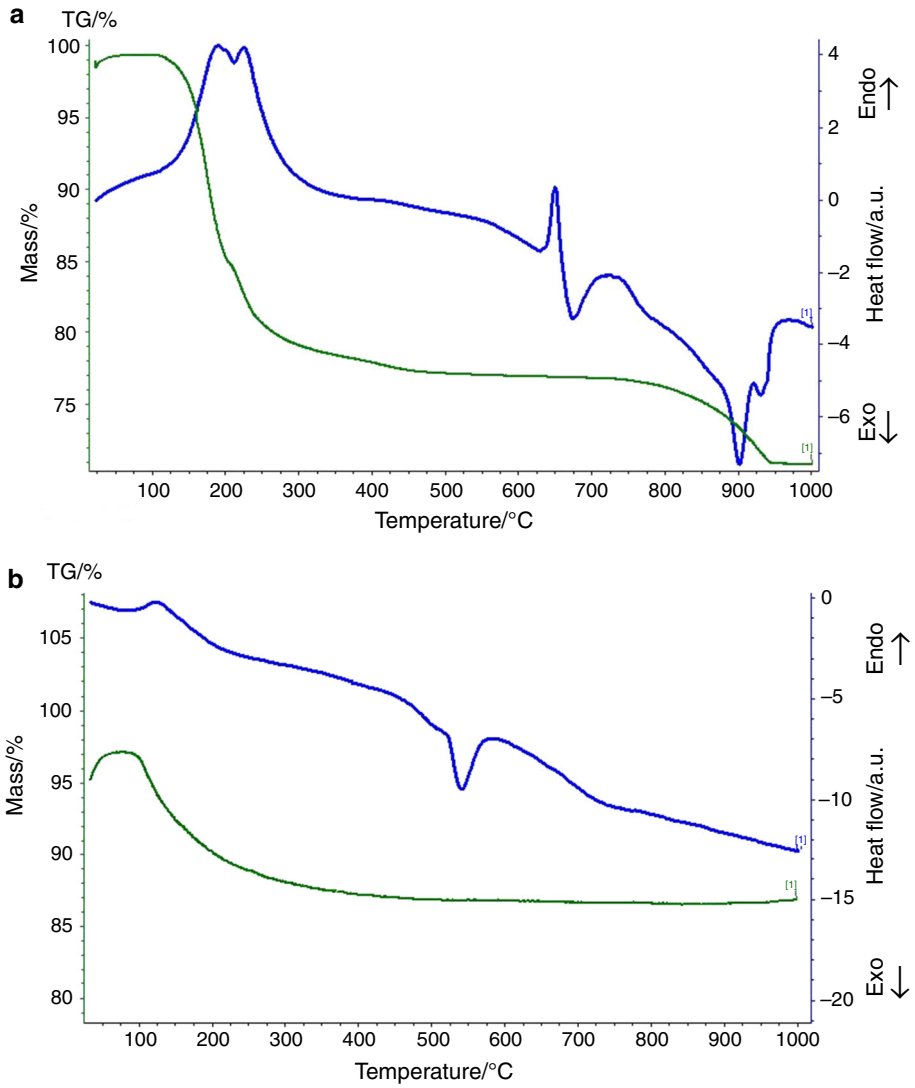

Fig. 9 Thermal analysis (DSC) results of sample S_1 (**a**), and S_2 (**b**) after milling

revealed below 300 °C, which are related to the thermal decomposition and dehydration of boric acid [26, 27] and TG analysis shows that this occurrence led to an about 20 % mass loss. In fact, this shows that about 20 % mass increase might be occurred due to the moisture sorption during mixing and before TG analysis. The third endothermic peak revealed at about 640 °C is related to the melting peak of Mg. This means that no reaction was taken place before the melting of Mg for the mixed powders as no exothermic peak could be seen in this range of temperature. Two exothermic reactions have occurred after the melting of Mg at about 670 and 900 °C, indicating that reaction (1) has occurred partially or completely in two steps for the sample S_1. As Mg is very prone to oxidation, the first exothermic peak could be related to the incomplete formation of MgO due to the exposure of Mg and B_2O_3 powders, and the second one might be related to the incomplete formation of B_4C. More importantly, a 6 % reduction in the mass value of the powders was revealed after 800 °C, in which the second exothermic reaction was taken place, which may show the formation of CO or CO_2 gases during this exothermic reaction, leading to an incomplete formation of the main products [47]. Figure 9b shows the thermal analysis of sample S_2. As this curve shows, milling of Mg and B_2O_3 for 1 h and then mechanical activation process in the presence of graphite powders for 4 h considerably change the thermal behavior of the Mg–B_2O_3–C ternary system during heating to 1000 °C. A weaker endothermic peak compared with the curve of sample S_1 was revealed below 200 °C, which shows that two-step milling processes might lead to the exit of moisture from the powders as only about 10 % mass reduction was taken place after this endothermic peak. As can be seen, an intensive exothermic reaction has occurred at about 520 °C, indicating that mechanical activation changed the synthesis mechanism of B_4C and MgO phases. It seems that

combustion synthesis has occurred in one step for this sample during an intensive exothermic reaction (see Fig. 9b, intensity of the DSC curve). No endothermic melting peak of Mg could be seen, meaning that MgO phase was completely formed during combustion synthesis at 520 °C. As can be seen, no reducing trend could be seen for TG analysis for this sample after combustion synthesis (520 °C), meaning that no CO and/or CO_2 gases may be formed for this sample. We believe that step 1 of mechanical activation was effective to make an adequate interface between B_2O_3 and Mg to make sure that all oxygen atoms were consumed for the formation of MgO phase. In fact, the milling of the ternary mixture without applying the first step of ball milling might lead to the presence and interference of carbon phase between Mg and B_2O_3 powders and a required interface between Mg ad B_2O_3 phases for complete formation of MgO might not be formed. While, for the sample S_2, during the formation of MgO, the exposure of fresh reduced boron to the C phase would lead to the formation of B_4C powders. In conclusion, it should be mentioned that mechanical activation in two steps could avoid the formation of unwanted phases after MACS process, and the reaction mechanism was changed after the mechanical activation that both the phases (B_4C and MgO) were completely formed in one step. In fact, the first step of the ball milling process for 1 h for sample S_2 (see Table 1) affected the kinetic of the reaction between Mg and B_2O_3, and the second step for 4 h changed the reaction mechanism of B_4C–MgO fabrication in solid state at a much lower temperature than 900 °C, indicating the simultaneous formation of MgO and B_4C phases.

In conclusion, the following mechanism could be suggested for fabrication of B_4C powders from the mechanically activated starting powders of Mg–B_2O_3–C:

1. MACS activates the magnesiothermic reaction between B_2O_3 and Mg, leading to the formation of liquid/gas (MgO) and liquid (B) reaction products, which the first step of the milling process between B_2O_3 and Mg highly affects this step.
2. The gaseous products of the reaction between B_2O_3 and Mg might activate the graphite powders, leading to their reaction with liquid boron to form B_4C particles with a small average particle size in a matrix of MgO phase. Finally, the leaching process removes the MgO matrix and submicron powders of B_4C phase with a low crystallite size of about 114 nm were formed.

Conclusions

In this study, microwave energy was used to stimulate the as-mixed and mechanically activated ternary system of B_2O_3–Mg–C powders for the final synthesis of B_4C powders from acid leaching of B_4C–MgO products, obtained via the MACS process. The following results could be drawn from the experimental results:

1. No MACS has occurred for the as-mixed ternary system, indicating that mechanical activation is required for the synthesis of B_4C–MgO phases.
2. Based on the XRD results, no phase change has occurred after two-step mechanical activation process, indicating that the ball milling parameters were chosen correctly to increase the surface contact between the powders and their energy levels without revealing new phase peaks in XRD patterns.
3. From XRD results, B_4C and MgO phases were formed after MACS without any detection of the corresponding peaks of the starting powders. Acid leaching by using HCl was also successful for the complete removal of MgO phase.
4. Pure B_4C powders with a submicron particles size and almost the spherical shape and an average crystallite size of 114 nm were obtained after MACS, followed by acid leaching.
5. From TG analysis, two-step mechanical activation process (first, ball milling of B_2O_3 and Mg, and second, addition of graphite powders) was effective to avoid the formation of unwanted gaseous products after MACS.
6. From DSC analysis, mechanical activation of the starting powders changed the reaction mechanism, in which combustion synthesis has occurred during one intensive reaction at solid state below 600 °C. In fact, a sharp reduction in reaction temperature has occurred in DSC analysis after mechanical activation.
7. It is finally proposed that liquid/gas (MgO) and liquid (B) fabricated after the reaction between B_2O_3 and Mg and the gaseous products of this reaction might stimulate the C phase for the reaction with liquid boron to form B_4C.

References

1. Suri A, Subramanian C, Sonber J, Murthy TC. Synthesis and consolidation of boron carbide: a review. Int Mater Rev. 2010;55(1):4–40.
2. Karandikar P, Evans G, Wong S, Aghajanian M, Sennett M. A review of ceramics for armor applications. Adv Ceram Armor IV Ceram Eng Sci Proc. 2009;29(6):163–75.
3. Lee H, Speyer RF. Pressureless sintering of boron carbide. J Am Ceram Soc. 2003;86(9):1468–73.
4. Mondal S, Banthia AK. Low-temperature synthetic route for boron carbide. J Eur Ceram Soc. 2005;25(2):287–91.
5. Dodd S, Saunders G, James B. Temperature and pressure dependences of the elastic properties of ceramic boron carbide (B_4C). J Mater Sci. 2002;37(13):2731–6.

6. Gosset D, Provot B. Boron carbide as a potential inert matrix: an evaluation. Prog Nucl Energy. 2001;38(3):263–6.
7. Lee J, Won C, Joo S, Maeng D, Kim H. Preparation of B_4C powder from B_2O_3 oxide by SHS process. J Mater Sci Lett. 2000;19(11):951–4.
8. Sharifi EM, Karimzadeh F, Enayati M. Mechanochemical assisted synthesis of B_4C nanoparticles. Adv Powder Technol. 2011;22(3):354–8.
9. Chen S, Wang D, Huang J, Ren Z. Synthesis and characterization of boron carbide nanoparticles. Appl Phys A. 2004;79(7):1757–9.
10. Hadian A, Bigdeloo J. The effect of time, temperature and composition on boron carbide synthesis by sol–gel method. J Mater Eng Perform. 2008;17(1):44–9.
11. Nikzad L, Ebadzadeh T, Vaezi M, Tayebifard A. Effect of milling on the combustion synthesis of ternary system B_2O_3, Mg and C. Micro Nano Lett IET. 2012;7(4):366–9.
12. Alizadeh A, Taheri-Nassaj E, Ehsani N. Synthesis of boron carbide powder by a carbothermic reduction method. J Eur Ceram Soc. 2004;24(10):3227–34.
13. Kobayashi T, Yoshida K, Yano T. Effects of heat-treatment temperature and starting composition on morphology of boron carbide particles synthesized by carbothermal reduction. Ceram Int. 2013;39(1):597–603.
14. Alkan M, Sonmez MS, Derin B, Yücel O. Effect of initial composition on boron carbide production by SHS process followed by acid leaching. Solid State Sci. 2012;14(11):1688–91.
15. Deng F, Xie H-Y, Wang L. Synthesis of submicron B_4C by mechanochemical method. Mater Lett. 2006;60(13):1771–3.
16. Jiang G, Xu J, Zhuang H, Li W. Fabrication of B_4C from $Na_2B_4O_7$+ Mg+ C by SHS method. Ceram Int. 2011;37(5):1689–91.
17. Wieczorek-Ciurowa K, Gamrat K. Mechanochemical syntheses as an example of green processes. J Therm Anal Calorim. 2007;88(1):213–7.
18. Filipek E, Wieczorek-Ciurowa K. Comparison between the synthesis in molybdenum and antimony oxides system by high-temperature treatment and high-energy ball milling. J Therm Anal Calorim. 2009;97(1):105–10.
19. Suryanarayana C. Mechanical alloying and milling. Prog Mater Sci. 2001;46(1):1–184.
20. Martos M, Morales J, Sanchez L. Mechanochemical synthesis of $Sn_{1-x}Mo_xO_2$ anode materials for Li-ion batteries. J Mater Chem. 2002;12(10):2979–84.
21. Mousavian RT, Sharafi S, Shariat M. Preparation of nano-structural Al_2O_3–TiB_2 in situ composite using mechanically activated combustion synthesis followed by intensive milling. Iran J Mater Sci Eng. 2011;8(2):1–9.
22. Mosleh A, Ehteshamzadeh M, Mousavian RT. Fabrication of an r-Al_2Ti intermetallic matrix composite reinforced with α-Al_2O_3 ceramic by discontinuous mechanical milling for thermite reaction. Int J Miner Metall Mater. 2014;21(10):1037–43.
23. Shishkovsky I, Scherbakov V, Morozov Y, Kuznetsov M, Parkin I. Surface Laser Sintering of exothermic powder compositions. J Therm Anal Calorim. 2008;91(2):427–36.
24. Hasani S, Panjepour M, Shamanian M. Effect of atmosphere and heating rate on mechanism of $MoSi_2$ formation during self-propagating high-temperature synthesis. J Therm Anal Calorim. 2012;107(3):1073–81.
25. Wang T, Liu R, Zhu M, Zhang J. Activation energy of self-heating process studied by DSC. J Therm Anal Calorim. 2002;70(2):507–19.
26. Mousavian RT, Sharafi S, Roshan M, Shariat M. Effect of mechanical activation of reagents' mixture on the high-temperature synthesis of Al_2O_3–TiB_2 composite powder. J Therm Anal Calorim. 2011;104(3):1063–70.
27. Mousavian RT, Sharafi S, Shariat M. Microwave-assisted combustion synthesis in a mechanically activated Al–TiO_2–H_3BO_3 system. Int J Refract Metal Hard Mater. 2011;29(2):281–8.
28. Siegert B, Comet M, Muller O, Pourroy G, Spitzer D. Reduced-sensitivity nanothermites containing manganese oxide filled carbon nanofibers. J Phys Chem C. 2010;114(46):19562–8.
29. Mousavian RT, Azizi N, Jiang Z, Boostani AF. Effect of Fe_2O_3 as an accelerator on the reaction mechanism of Al–TiO_2 nanothermite system. J Therm Anal Calorim. 2014;117:1–9.
30. Deris L, Sharafi S, Akbari G. Effect of milling speed on mechanical activation of Al/ZrO_2/H_3BO_3 system to prepare Al_2O_3–ZrB_2 composite powder. J Therm Anal Calorim. 2014;115(1):401–7.
31. Assis R, Bomio M, Nascimento R, Paskocimas C, Longo E, Motta F. Rapid calcination of ferrite $Ni_{0.}$ $_{75}Zn_{0.}$ $_{25}Fe_2O_4$ by microwave energy. J Therm Anal Calorim. 2014;118(1):277–85.
32. Oberti TG, Alessandrini JL, Susana Cortizo M. Thermal characterization of novel *p*-nitrobenzylacrylate–diisopropyl fumarate copolymer synthesized under microwave energy. J Therm Anal Calorim. 2012;109(3):1525–31.
33. Borkar S, Dharwadkar S. Temperatures and kinetics of anatase to rutile transformation in doped TiO_2 heated in microwave field. J Therm Anal Calorim. 2004;78(3):761–7.
34. Szepes A, Fiebig A, Ulrich J, Szabó-Révész P. Structural study of α-lactose monohydrate subjected to microwave irradiation. J Therm Anal Calorim. 2007;89(3):757–60.
35. Maul J, Brito A, de Oliveira A, Lima S, Maurera M, Keyson D, et al. Influence of the synthesis media in the properties of CuO obtained by microwave-assisted hydrothermal method. J Therm Anal Calorim. 2011;106(2):519–23.
36. Guiotoku M, Rambo CR, Hotza D. Charcoal produced from cellulosic raw materials by microwave-assisted hydrothermal carbonization. J Therm Anal Calorim. 2014;117:1–7.
37. Satapathy L, Ramesh P, Agrawal D, Roy R. Microwave synthesis of phase-pure, fine silicon carbide powder. Mater Res Bull. 2005;40(10):1871–82.
38. Ganesh I, Johnson R, Rao G, Mahajan Y, Madavendra S, Reddy B. Microwave-assisted combustion synthesis of nanocrystalline $MgAl_2O_4$ spinel powder. Ceram Int. 2005;31(1):67–74.
39. Comet M, Pichot V, Siegert B, Fousson E, Mory J, Moitrier F, et al. Preparation of Cr_2O_3 nanoparticles for superthermites by the detonation of an explosive nanocomposite material. J Nanopart Res. 2011;13(5):1961–9.
40. Comet M, Pichot V, Siegert B, Spitzer D, Moeglin JP, Boehrer Y. Use of nanodiamonds as a reducing agent in a chlorate-based energetic composition. Propellants Explos Pyrotech. 2009;34(2):166–73.
41. Yaghoubi M, Torabi O. Effect of the magnesium content on the mechanochemical behavior in ternary system Mg–B_2O_3–C. Int J Refract Metal Hard Mater. 2014;43:132–40.
42. Jung C-H, Lee M-J, Kim C-J. Preparation of carbon-free B_4C powder from B_2O_3 oxide by carbothermal reduction process. Mater Lett. 2004;58(5):609–14.
43. Marinca TF, Neamţu BV, Chicinaş I, Pascuta P. Influence of mechanical activation time, annealing, and Fe/O ratio on Fe_3O_4/Fe composites formation from Fe_2O_3 and Fe powders mixture. J Therm Anal Calorim. 2014;118(2):1245–51.
44. Kostova B, Petkova V. Effect of high-energy milling and thermal treatment on the solid-phase reactions in apatite–ammonium sulphate system. J Therm Anal Calorim. 2014;116(2):737–46.
45. Wieczorek-Ciurowa K, Gamrat K. NiAl/Ni_3Al–Al_2O_3 composite formation by reactive ball milling. J Therm Anal Calorim. 2005;82(3):719–24.
46. Wieczorek-Ciurowa K, Gamrat K, Paryło M, Shirokov JG. The influence of aluminium and aluminium oxide on the effects of mechanical activation of nickel hydroxocarbonate. J Therm Anal Calorim. 2002;69(1):237–43.
47. Mohanty R, Balasubramanian K, Seshadri S. Multiphase formation of boron carbide in B_2O_3–Mg–C based micropyretic process. J Alloy Compd. 2007;441(1):85–93.